ELSEVIER

Ceramics International 32 (2006) 539–543

CERAMICS INTERNATIONAL

www.elsevier.com/locate/ceramint

Perovskite stabilization and dielectric properties of $Mg_{1/3}Nb_{2/3}$-substituted $Pb[(Zn_{1/3}Ta_{2/3}),Ti]O_3$

Jee-Su Kim, Nam-Kyoung Kim *

Department of Inorganic Materials Engineering, Kyungpook National University, E8-424, 1370 Sankyuk-Dong, Buk-Gu, Daegu 702-701, Korea

Received 10 February 2005; received in revised form 25 February 2005; accepted 16 April 2005
Available online 9 June 2005

Abstract

An amount of 20 mol% $(Mg_{1/3}Nb_{2/3})O_2$ was replaced into the octahedral sites of $Pb(Zn_{1/3}Ta_{2/3})O_3$ (PZTa)–$PbTiO_3$ (PT) and resultant changes in the perovskite stabilization and dielectric properties were examined. Perovskite formation at the $Pb(Zn_{1/3}Ta_{2/3})O_3$-rich compositions (where the pyrochlore phase is prone to develop) turned out to improve substantially by the compositional modification. Tetragonality factors increased continuously with increasing fractions of $PbTiO_3$. Maximum dielectric constant values were much higher than those without the $(Mg_{1/3}Nb_{2/3})O_2$ substitution.

Keywords: A. Powders: solid state reaction; B. X-ray methods; C. Dielectric properties; Ceramics; Perovskite oxides

1. Introduction

Lead magnesium niobate $Pb(Mg_{1/3}Nb_{2/3})O_3$ (PMN) is a typical complex-perovskite relaxor, exhibiting frequency-dependent dielectric relaxation with diffuse phase transition modes in the dielectric constant spectra [1–5]. In contrast, lead zinc tantalate $Pb(Zn_{1/3}Ta_{2/3})O_3$ (PZTa), tantalum analog of $Pb(Zn_{1/3}Nb_{2/3})O_3$ (PZN), has not been synthesized to a perovskite structure by any means yet [5–12], although the stoichiometry of $Pb(B_{1/3}^{2+}B_{2/3}^{5+})O_3$ is identical. Meanwhile, lead titanate $PbTiO_3$ (PT) is also a perovskite compound, but with sharp modes in the phase transition. Perovskite PMN and PT can be prepared quite readily through direct reaction among constituent components, in contrast to the reported difficulties in PZTa.

To date, several compositional modifications in the octahedral lattice sites of PZTa have been attempted to stabilize the perovskite structure by Ti [10], $Mg_{1/3}Ta_{2/3}$ [8], $Mg_{1/3}Nb_{2/3}$ [5], $Fe_{1/2}Ta_{1/2}$ [11], and $Fe_{1/2}Nb_{1/2}$ [12]. Among the various substituents, Ti was the most effective (and $Mg_{1/3}Nb_{2/3}$ the second) one in suppressing the pyrochlore formation [10]. Meanwhile, complete (≥99%) development of the perovskite structure in pseudobinary PZTa-PT was achieved only when the fraction of PT was ≥ 60 mol% [10]. In the present study, therefore, a substantial fraction (20 mol%) of PMN was additionally introduced into PZTa–PT and consequent perovskite formation and resultant dielectric properties were investigated. In order to further assist the perovskite stabilization, a B-site precursor method [13] (conceptually identical to the columbite process [14,15]) was employed in powder preparation.

2. Experimental

The investigated system can be expressed as $(0.8 - x)PZTa - 0.2PMN - xPT$, i.e. $Pb[(Zn_{1/3}Ta_{2/3})_{0.8-x}(Mg_{1/3}Nb_{2/3})_{0.2}Ti_x]O_3$ (or PZTMNT in short). Source materials used were high-purity oxide chemicals of PbO (99.5%), ZnO (99.8%), Ta_2O_5 (99.9%), MgO (99.9%), Nb_2O_5 (99.9%), and TiO_2 (99.9%). Stoichiometries of the B-site precursor $[(Zn_{1/3}Ta_{2/3})_{0.8-x}(Mg_{1/3}Nb_{2/3})_{0.2}Ti_x]O_2$ and PZTMNT systems were maintained as close

* Corresponding author. Tel.: +82 53 950 5636; fax: +82 53 950 5645.
E-mail address: nkkim@knu.ac.kr (N.-K. Kim).

0272-8842/$30.00
doi:10.1016/j.ceramint.2005.04.008

to the nominal values as possible by moisture compensation of the raw chemicals as well as of the synthesized precursor powders.

Powder batches of constituent chemicals were milled under ethyl alcohol (ZrO_2 media) for 12 h, dried overnight, and calcined at 1150–1250 °C (depending on composition) for 2 h for the formation of precursor phases. The milling, drying, and calcination procedures were repeated one more time at identical conditions to enhance the phase development. After the addition of PbO in stoichiometric proportions (i.e. without any excess amount), the powders were milled, dried, and calcined at 850 °C for 2 h, followed by additional milling to calcination (850–1000 °C, 2 h) steps to promote perovskite formation. Prepared powders were examined by X-ray diffraction (XRD) to identify the phases formed. The powders were then isostatically pressed into pellet-type preforms and densified at 1050–1250 °C for 1 h in a multiple-enclosure crucible setup to minimize lead-loss during exposure to high temperatures. Major faces of the sintered specimens were ground/polished and bulk densities were determined geometrically. After gold-sputtering for electrical contacts, temperature-dependent dielectric constant values were measured using an impedance analyzer under weak-field (~1 V_{rms}/mm) low-frequency (1 kHz to 1 MHz) conditions. The samples were fractured, gold-coated, and microstructures were examined using a scanning electron microscope (SEM).

3. Results and discussion

X-ray diffraction patterns of the B-site precursor $[(Zn_{1/3}Ta_{2/3})_{0.8-x}(Mg_{1/3}Nb_{2/3})_{0.2}Ti_x]O_2$ are shown in Fig. 1. The pattern of $x = 0.0$ (i.e. $[(Zn_{1/3}Ta_{2/3})_{0.8}(Mg_{1/3}Nb_{2/3})_{0.2}]O_2$) matched that of the tri-αPbO_2 structure ($ZnTa_2O_6$, ICDD No. 39-1484), which indicates that the 20 mol% component of $(Mg_{1/3}Nb_{2/3})O_2$ (columbite structure, ICDD No. 33-875) had been totally dissolved into the host structure of tri-αPbO_2. The tri-αPbO_2 structure was also observed at $x = 0.2$. In contrast, the structure of $x = 0.8$ (i.e. $[(Mg_{1/3}Nb_{2/3})_{0.2}Ti_{0.8}]O_2$) could be identified as rutile. However, the observed pattern was neither TiO_2 (rutile, ICDD No. 21-1276), nor $[(Mg_{1/3}Nb_{2/3})_{1/2}Ti_{1/2}]O_2$ (rutile, ICDD No. 40-366). Instead the pattern seemed closer to that of a rutile solid solution (formed theoretically as $0.4[(Mg_{1/3}Nb_{2/3})_{1/2}Ti_{1/2}]O_2 + 0.6TiO_2$), judging from careful comparison of the diffraction angles. Likewise, the rutile (detected down to $x = 0.2$) seemed to be solid solutions formed between TiO_2 and $[(B'_{1/3}B''_{2/3})_{1/2}Ti_{1/2}]O_2$ (where $B' = Mg$ and/or Zn and $B'' = Ta$ and/or Nb). As a whole, continuous solubilities did not develop in the entire B-site precursor system due probably to the totally dissimilar structures of the end components, hence resulting in coexistence of the two structures (at only an intermediate composition of $x = 0.2$). By considering relative intensities, the solubility limit of the rutile in the host tri-αPbO_2 structure could be estimated as $0.0 \ll x < 0.2$, whereas the limit of the

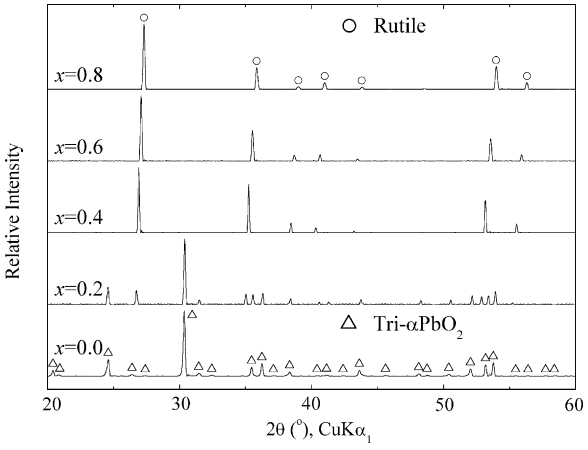

Fig. 1. Developed structures in the B-site precursor system $[(Zn_{1/3}Ta_{2/3})_{0.8-x}(Mg_{1/3}Nb_{2/3})_{0.2}Ti_x]O_2$.

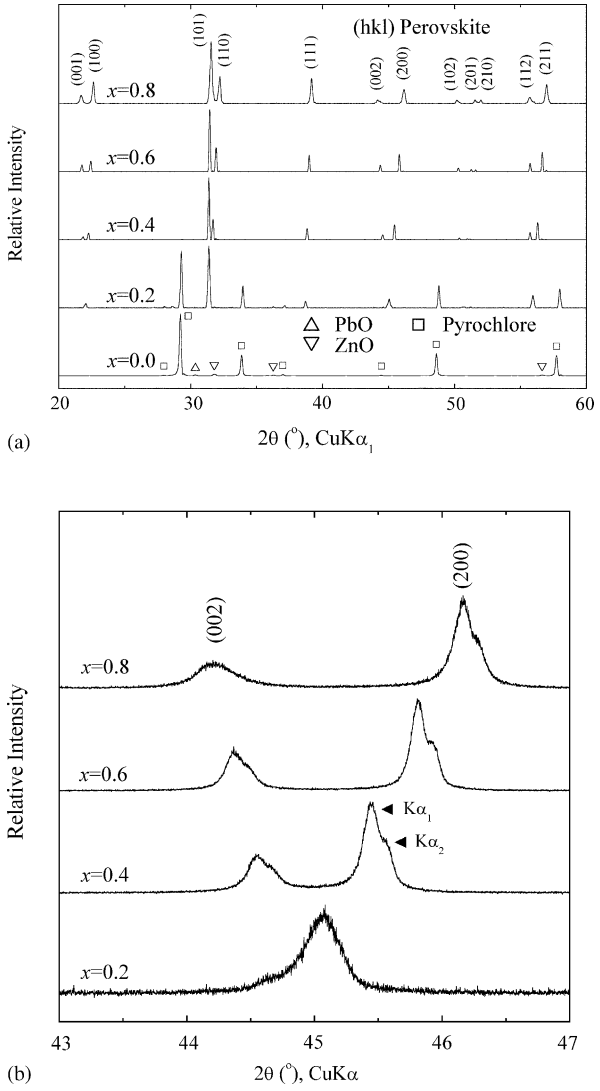

Fig. 2. X-ray diffraction patterns of the $Pb[(Zn_{1/3}Ta_{2/3})_{0.8-x}(Mg_{1/3}Nb_{2/3})_{0.2}Ti_x]O_3$ system (a) with an enlarged view around 45° (b).

tri-αPbO_2 in the rutile matrix seemed to be $0.2 \ll x < 0.4$. Meanwhile, the diffraction angles increased gradually with increasing values of x, which will be discussed later.

XRD spectra of the $(0.8 - x)$PZTa $-$ 0.2PMN $- x$PT system are displayed in Fig. 2(a), where the (h k l) indexing is based on a tetragonal symmetry of a perovskite structure. The pattern of $x = 0.0$ (i.e. 0.8PZTa $-$ 0.2PMN) was basically of a cubic pyrochlore (ICDD No. 34-395) without any trace of the perovskite structure (along with negligible fractions of PbO and ZnO), indicating that introduction of 20 mol% PMN is still insufficient for the perovskite development. A perovskite then appeared suddenly at $x = 0.2$ and became the sole structure identified at higher values of x, which is attributed undoubtedly to the increased fractions of PT. In addition, a tetragonal symmetry of the perovskite developed more pronouncedly, Fig. 2(b), with further increase in x. It is quite interesting to note that the composition range (where the pyrochlore and the perovskite coexisted) coincides approximately with the phase boundary of tri-αPbO_2 and rutile (Fig. 1). It can be concluded, at least in the present study, that the perovskite forms rather easily from the B-site precursor of a rutile structure (which is well known), whereas the pyrochlore is prone to develop from the tri-αPbO_2 precursor.

Tetragonal lattice parameters of the perovskite structure were determined from the diffraction angles and the results are presented in Fig. 3. The a parameter decreased progressively with increasing values of x (PT fractions), whereas the c parameter increased roughly symmetrically. Hence the tetragonality factors (c/a) increased continuously from 1.006 ($x = 0.2$) to 1.043 ($x = 0.8$). This increase is directly induced by the incorporation of PT ($c/a = 1.065$, ICDD No. 6-452). Meanwhile the average lattice parameters of $(a^2c)^{1/3}$ decreased steadily from 0.4016 to 0.3984 nm in the same composition range. The decrease is undoubtedly associated with the gradual contraction of the unit cell dimension by replacement of the octahedral $Zn_{1/3}Ta_{2/3}$ complex by Ti, effective ionic radii [16] of which are 0.0673 nm (weight-averaged value) and 0.0605 nm, respectively. Therefore, the diffraction angles were observed to

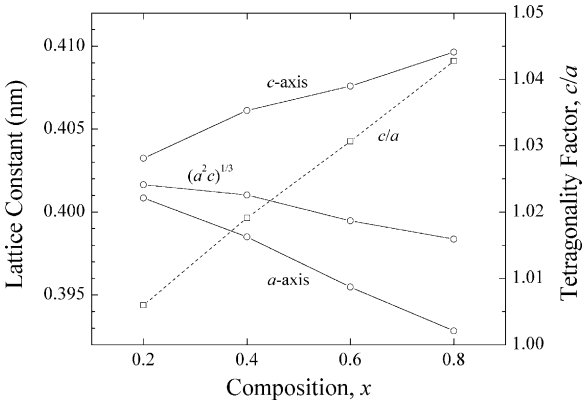

Fig. 3. Lattice parameters of the perovskite structure and tetragonality factors of the $(0.8 - x)$PZTa $-$ 0.2PMN $- x$PT system.

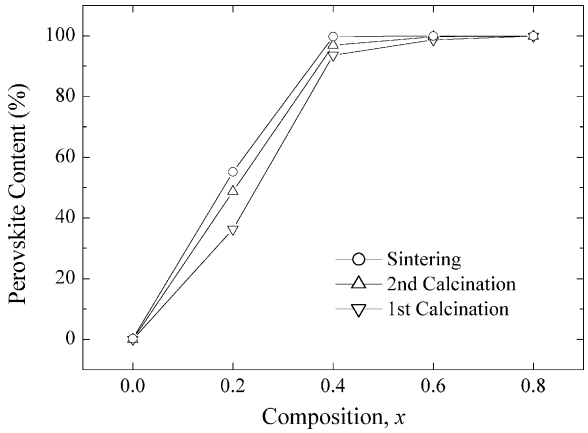

Fig. 4. Perovskite contents of the $(0.8 - x)$PZTa $-$ 0.2PMN $- x$PT system.

increase continuously with increasing values of x, Figs. 1 and 2(a). Relative densities of the sintered ceramics were 94–96% of theoretical.

Perovskite formation yields in the PZTMNT system, estimated by quantitative comparison between the perovskite and pyrochlore peaks of highest intensities as $I_{Perov.}/(I_{Perov.} + I_{Pyro.})$, are plotted in Fig. 4. In general, the

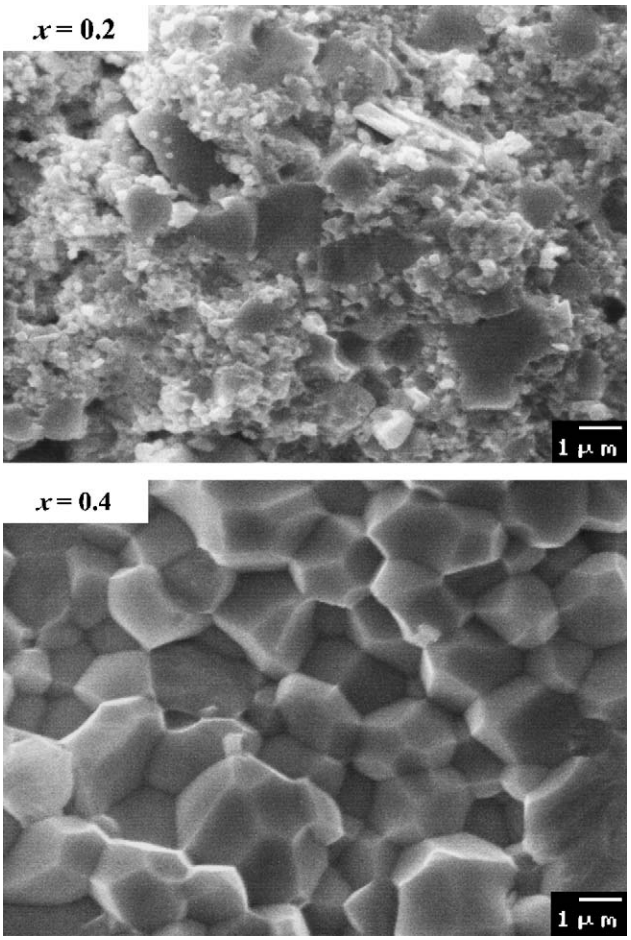

Fig. 5. SEM images of the fractured ceramics of selected compositions.

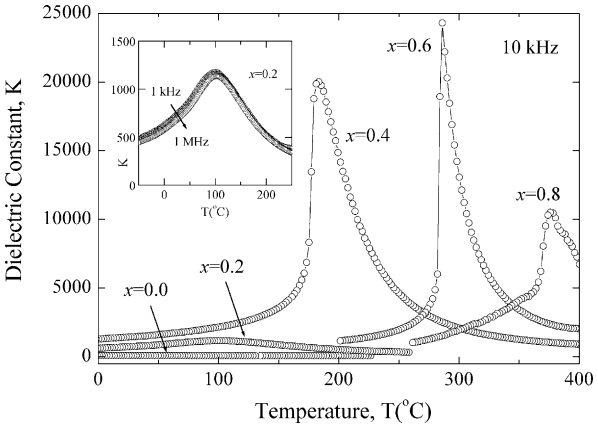

Fig. 6. Temperature dependence of the dielectric constant.

perovskite contents increased gradually with the heat-treatment stages: e.g. 36, 49, and 55% after first and second calcination and after sintering ($x = 0.2$). Meanwhile, the value of 0% (even after sintering) at $x = 0.0$ increased rapidly to 100% ($x = 0.4$), as discussed in Fig. 2(a). When the results are compared with those of the PZTa–PT system [10], the perovskite yields turned out to improve substantially due to the active role of substituted PMN. Nevertheless, complete stabilization of the perovskite structure in the entire composition range was not accomplished, especially at PZTa-rich compositions.

Fractomicrographs of the ceramics of selected compositions are displayed in Fig. 5. The image of $x = 0.0$ (not shown) was mostly of small pyrochlore grains, whereas that of $x = 0.2$ consisted of larger perovskite grains scattered in the pyrochlore matrix. In contrast, well-developed polyhedral perovskite grains were observed at $x = 0.4$ with intergranular fracture modes. The micrographs of $x = 0.6$ and 0.8 (not shown) were almost identical to that of $x = 0.4$, except for somewhat different grain sizes. The microstructure constitutions are generally consistent with the perovskite development results, Fig. 4.

Dielectric constant values of the ceramics are contrasted in Fig. 6 with frequency dependence for $x = 0.2$ (inset). The dielectric constant of $x = 0.0$ changed only linearly in the covered temperature range without any development of dielectric maxima. Room-temperature values were 76–78 with gradients of −680 to −670 ppm/K in the entire frequency range. The maximum peaks started to appear at $x = 0.2$, where magnitudes of the peaks (maximum dielectric constants) were still quite low (e.g. 1160 at 10 kHz) due to the presence of pyrochlore (45%). Nevertheless, typical behavior of frequency-dependent dielectric relaxation is well demonstrated. The rather broad phase transitions then changed to sharp ones with maximum values rising steeply to 20,000 ($x = 0.4$) and 24,500 ($x = 0.6$), where the dielectric relaxation behavior could hardly be observed any more. The dielectric maximum temperatures (T_{max}) increased linearly from 100 °C ($x = 0.2$) to 377 °C ($x = 0.8$) at 10 kHz. Degree of the temperature shift with frequency change ($T_{max,1\ MHz} - T_{max,1\ kHz}$) was 4 °C at $x = 0.2$, which decreased to negligible values (<1 °C) at higher values of x. Similar changes in the phase transition modes of diffuse to sharp ones were also reported in many $Pb(B_{1/3}^{2+}B_{2/3}^{5+})O_3$–$PbTiO_3$ ceramics, including PZTa–PT [10].

4. Summary

In the B-site precursor $[(Zn_{1/3}Ta_{2/3})_{0.8-x}(Mg_{1/3}Nb_{2/3})_{0.2}Ti_x]O_2$, tri-$\alpha PbO_2$ and rutile structures were detected at $x \leq 0.2$ and $0.2 \leq x$, respectively, with the two structures coexisting at an intermediate composition of $x = 0.2$. In $(0.8 - x)$PZTa−0.2PMN − xPT, a perovskite structure started to develop at $x = 0.2$ and became the predominant one at $0.4 \leq x$. Hence, the perovskite formation was improved significantly (especially in the PZTa-rich compositions) by the introduction of 20 mol% PMN. With increasing fractions of PT, tetragonal symmetries of the perovskite structure developed progressively, whereas unit cell volumes decreased steadily. Maximum dielectric constant values of the investigated PZTMNT system were much higher than those of PZTa–PT (i.e. without the PMN substitution). In contrast, the dielectric maximum temperature ranges were reduced somewhat by the incorporation of PMN. Meanwhile, phase transition modes (reflected in the dielectric constant spectra) were rather broad at $x = 0.2$, but became quite sharp at higher values of x.

Acknowledgement

This study was supported by a Korea Research Foundation Grant (KRF-2001-041-E00456).

References

[1] I.G. Ismailzade, An X-Ray study of the $Pb_3NiNb_2O_9$–$Pb_3MgNb_2O_9$ system, Sov. Phys. Crystallogr. 5 (2) (1960) 292–293.
[2] K. Katayama, M. Abe, T. Akiba, H. Yanagida, Sintering and dielectric properties of single-phase $Pb(Mg_{1/3}Nb_{2/3})O_3$–$PbTiO_3$, J. Eur. Ceram. Soc. 5 (3) (1989) 183–191.
[3] Y. Yamashita, Relaxor ceramic dielectric materials for multilayer ceramic capacitors, in: Proceedings of the Seventh IEEE International Symposium on Applications of Ferroelectrics, 1990, pp. 241–245.
[4] M.-C. Chae, N.-K. Kim, Perovskite formation by B-site precursor method and dielectric characteristics of $Pb[Mg_{1/3}(Ta,Nb)_{2/3}]O_3$ ceramic system, Ferroelectrics 209 (34) (1998) 603–613.
[5] M.-C. Chae, S.-M. Lim, N.-K. Kim, Stabilization of perovskite phase and enhancement in dielectric properties by substitution of $Pb(Mg_{1/3}Nb_{2/3})O_3$ to $Pb(Zn_{1/3}Ta_{2/3})O_3$, Ferroelectrics 242 (1–4) (2000) 25–35.
[6] T.R. Shrout, A. Halliyal, Preparation of lead-based ferroelectric relaxors for capacitors, Am. Ceram. Soc. Bull. 66 (4) (1987) 704–711.

[7] H.C. Ling, M.F. Yan, W.W. Rhodes, Phase stability in $Pb(B'_{1/2}B''_{1/2})O_3$ and $Pb(B'_{1/3}B''_{2/3})O_3$ compositions, Ferroelectrics 89 (1989) 69–80.
[8] S.-M. Lim, N.-K. Kim, Perovskite phase developments in $Pb[(Mg,Zn)_{1/3}Ta_{2/3}]O_3$ system and dielectric characteristics, J. Mater. Sci. 35 (17) (2000) 4373–4378.
[9] B.-Y. Ahn, N.-K. Kim, Perovskite phase developments and dielectric characteristics in barium-substituted lead zinc tantalate system, Mater. Res. Bull. 35 (10) (2000) 1677–1687.
[10] J.-S. Kim, N.-K. Kim, H. Kim, Perovskite formation and dielectric characteristics of $Pb(Zn_{1/3}Ta_{2/3})O_3$ with $PbTiO_3$ substitution, J. Am. Ceram. Soc. 86 (6) (2003) 929–933.
[11] J.-A. Lee, N.-K. Kim, Development of perovskite in Fe-substituted $Pb(Zn_{1/3}Ta_{2/3})O_3$ and dielectric characteristics, Mater. Res. Bull., in press.
[12] J.-A. Lee, N.-K. Kim, Perovskite formation and dielectric properties of $Pb[(Zn_{1/3}Ta_{2/3}),(Fe_{1/2}Nb_{1/2})]O_3$, Mater. Lett. 59 (1) (2005) 32–35.
[13] B.-H. Lee, N.-K. Kim, J.-J. Kim, S.-H. Cho, Perovskite formation sequence by B-site precursor method and dielectric properties of PFW-PFN ceramics, Ferroelectrics 211 (1–4) (1998) 233–247.
[14] S.L. Swartz, T.R. Shrout, Fabrication of perovskite lead magnesium niobate, Mater. Res. Bull. 17 (10) (1982) 1245–1250.
[15] S.L. Swartz, T.R. Shrout, W.A. Schulze, L.E. Cross, Dielectric properties of lead magnesium niobate ceramics, J. Am. Ceram. Soc. 67 (5) (1984) 311–315.
[16] R.D. Shannon, Revised effective ionic radii and systematic studies of interatomic distances in halides and chalcogenides, Acta Crystallogr. A32 (5) (1976) 751–767.